



Since January 2020 Elsevier has created a COVID-19 resource centre with free information in English and Mandarin on the novel coronavirus COVID-19. The COVID-19 resource centre is hosted on Elsevier Connect, the company's public news and information website.

Elsevier hereby grants permission to make all its COVID-19-related research that is available on the COVID-19 resource centre - including this research content - immediately available in PubMed Central and other publicly funded repositories, such as the WHO COVID database with rights for unrestricted research re-use and analyses in any form or by any means with acknowledgement of the original source. These permissions are granted for free by Elsevier for as long as the COVID-19 resource centre remains active.



Development of flexible electrochemical impedance spectroscopy-based biosensing platform for rapid screening of SARS-CoV-2 inhibitors

Lik-Voon Kiew^{a,b,1}, Chia-Yu Chang^{b,c,1}, Sheng-Yu Huang^{d,e,f,1}, Pei-Wen Wang^{g,h}, Choon-Han Hehⁱ, Chung-Te Liu^{j,k}, Chia-Hsin Cheng^b, Yi-Xiang Lu^b, Yen-Chen Chen^b, Yi-Xuan Huang^b, Sheng-Yun Chang^{d,e,f,1}, Huei-Yu Tsai^g, Yu-An Kung^{d,e,f}, Peng-Nien Huang^{d,e,f}, Ming-Hua Hsu^m, Bey-Fen Leoⁿ, Yiing-Yee Foo^a, Chien-Hao Su^b, Kuo-Chen Hsu^o, Po-Hsun Huang^{p,q}, Chirk-Jenn Ng^r, Adeeba Kamarulzaman^s, Chiun-Jye Yuan^{b,t}, Dar-Bin Shieh^{g,h,u}, Shin-Ru Shih^{d,e,f,**}, Lip-Yong Chung^{i,***}, Chia-Ching Chang^{b,c,v,w,*}

^a Department of Pharmacology, Faculty of Medicine, University of Malaya, 50603, Kuala Lumpur, Malaysia

^b Department of Biological Science and Technology, College of Biological Science and Technology, National Yang Ming Chiao Tung University, Hsinchu, 30068, Taiwan

^c Center for Intelligent Drug Systems and Smart Bio-devices (IDS²B), National Yang Ming Chiao Tung University, Hsinchu, 30068, Taiwan

^d Research Center for Emerging Viral Infections, College of Medicine, Chang Gung University, Taoyuan, 33301, Taiwan

^e Department of Medical Biotechnology and Laboratory Science, College of Medicine, Chang Gung University, Taoyuan, 33301, Taiwan

^f Department of Laboratory Medicine, Linkou Chang Gung Memorial Hospital, Taoyuan, 33301, Taiwan

^g Institute of Oral Medicine and Department of Stomatology, College of Medicine, National Cheng Kung University Hospital, National Cheng Kung University, Tainan, 70101, Taiwan

^h Center of Applied Nanomedicine, National Cheng Kung University, Tainan, 70101, Taiwan

ⁱ Department of Pharmaceutical Chemistry, Faculty of Pharmacy, University of Malaya, 50603, Kuala Lumpur, Malaysia

^j Division of Nephrology, Department of Internal Medicine, Wan-Fang Hospital, Taipei Medical University, Taipei, 11696, Taiwan

^k Graduate Institute of Clinical Medicine, College of Medicine, Taipei Medical University, Taipei, 11031, Taiwan

^l Bachelor Program in Artificial Intelligence, Chang Gung University, Taoyuan, 33301, Taiwan

^m Department of Chemistry, National Changhua University of Education, Changhua, 50007, Taiwan

ⁿ Faculty of Medicine, University of Malaya, 50603, Kuala Lumpur, Malaysia

^o Pd Biomedical Co., Ltd., Taoyuan, 32560, Taiwan

^p Institute of Clinical Medicine, Cardiovascular Research Center, National Yang Ming Chiao Tung University, Taipei, 11121, Taiwan

^q Division of Cardiology, Taipei Veterans General Hospital, Taipei, 11217, Taiwan

^r Department of Primary Care Medicine, Faculty of Medicine, University of Malaya, 50603, Kuala Lumpur, Malaysia

^s Department of Medicine, Faculty of Medicine, University of Malaya, 50603, Kuala Lumpur, Malaysia

^t Institute of Molecular Medicine and Bioengineering, National Yang Ming Chiao Tung University, Hsinchu, 30068, Taiwan

^u Center for Micro/Nano Science and Technology, National Cheng Kung University, Tainan, 70101, Taiwan

^v Department of Electrophysics, National Yang Ming Chiao Tung University, Hsinchu, 30010, Taiwan

^w Institute of Physics, Academia Sinica, Nankang, Taipei, 11529, Taiwan

ARTICLE INFO

Keywords:

Palladium nano-thin-film electrode
Biosensor
Electrochemical impedance spectroscopy (EIS)
ACE2-SARS CoV 2 S-Protein interaction
SARS-CoV-2 infection inhibitors

ABSTRACT

Severe acute respiratory syndrome coronavirus 2 (SARS-CoV-2) enters the cells through the binding of its spike protein (S-protein) to the cell surface-expressing angiotensin-converting enzyme 2 (ACE2). Thus, inhibition of S-protein-ACE2 binding may impede SARS-CoV-2 cell entry and attenuate the progression of Coronavirus disease 2019 (COVID-19). In this study, an electrochemical impedance spectroscopy-based biosensing platform consisting of a recombinant ACE2-coated palladium nano-thin-film electrode as the core sensing element was fabricated for the screening of potential inhibitors against S-protein-ACE2 binding. The platform could detect

* Corresponding author. Department of Biological Science and Technology, College of Biological Science and Technology, National Yang Ming Chiao Tung University, Hsinchu, 30068, Taiwan.

** Corresponding author. Research Center for Emerging Viral Infections, College of Medicine, Chang Gung University, Taoyuan, 33301, Taiwan.

*** Corresponding author.

E-mail addresses: srshih@mail.cgu.edu.tw (S.-R. Shih), chungly@um.edu.my (L.-Y. Chung), cchang01@faculty.nctu.edu.tw (C.-C. Chang).

¹ These authors contributed equally to this work.

<https://doi.org/10.1016/j.bios.2021.113213>

Received 9 February 2021; Received in revised form 27 March 2021; Accepted 30 March 2021

Available online 3 April 2021

0956-5663/© 2021 The Author(s).

Published by Elsevier B.V. This is an open access article under the CC BY-NC-ND license

(<http://creativecommons.org/licenses/by-nc-nd/4.0/>).

interference of small analytes against S-protein-ACE2 binding at low analyte concentration and small volume (0.1 µg/mL and ~1 µL, estimated total analyte consumption < 4 pg) within 21 min. Thus, a few potential inhibitors of S-protein-ACE2 binding were identified. This includes (2S,3aS,6aS)-1-((S)-N-((S)-1-Carboxy-3-phenylpropyl)alanyl)tetrahydrocyclopenta[b] pyrrole-2-carboxylic acid (ramiprilat) and (2S,3aS,7aS)-1-[(2S)-2-[[[(2S)-1-Carboxybutyl]amino]propanoyl]-2,3,3a,4,5,6,7,7a-octahydroindole-2-carboxylic acid (perindoprilat) that reduced the binding affinity of S-protein to ACE2 by 72% and 67%; and SARS-CoV-2 *in vitro* infectivity to the ACE2-expressing human oral cavity squamous carcinoma cells (OEC-M1) by 36.4 and 20.1%, respectively, compared to the PBS control. These findings demonstrated the usefulness of the developed biosensing platform for the rapid screening of modulators for S-protein-ACE2 binding.

1. Introduction

Since December 2019, Severe acute respiratory syndrome coronavirus 2 (SARS-CoV-2) has infected more than 122 million people and caused over 2.7 million deaths worldwide (Dong et al., 2020). To curb the spread of the Coronavirus disease 2019 (COVID-19) pandemic, research and clinical communities have invested numerous efforts into repurposing the presently available drugs against the infection (Harri-son, 2020), and several potential therapeutic leads, including remdesivir, lopinavir-ritonavir combinations, chloroquine, and hydroxychloroquine, were enrolled in the WHO's Solidarity Therapeutics Trial (Singh et al., 2020). Despite the initial reports of success, a recent interim report released by the World Health Organization's Solidarity Therapeutics Trial concluded that remdesivir, hydroxychloroquine, lopinavir/ritonavir, and interferon regimens have little or no effect on 28-day mortality or the in-hospital course of COVID-19 among hospitalized patients (Pan et al., 2020), while the progression of other drug-repurposing activities was generally slow, although some are under clinical trials (Singh et al., 2020).

The technical complexity and high expense involved in screening new leads through conventional computational and biological experimental approaches are among the main factors that impede drug-repurposing efforts (Singh et al., 2020). This study reported the use of electrochemical impedance spectroscopy (EIS)-based biosensing techniques for the rapid screening of new therapeutic leads against SARS-CoV-2 infection from the pool of FDA-approved drugs, as a new alternative approach to conventional drug-repurposing approaches. EIS-based biosensing can detect interactions between bio-macromolecules with high sensitivity, selectivity, and reliability (Li et al., 2013; Rocheville et al., 2013; Tepeli and Ülkü 2018). The use of this technique in the studies of receptor-ligand interactions, drug screening (Kilic et al., 2018a, 2018b; Lundstrom 2017; Rocheville et al., 2013), viral protein detection (Li et al., 2013; Santos et al., 2018; Tepeli and Ülkü 2018), and cancer diagnosis (Chang et al., 2019a) has been increasing. This study hypothesized that this technique may be adopted to detect changes in the receptor-ligand interactions upon exposure to pharmacological inhibitors of such interactions.

Previous reports have found that SARS-CoV-2 spreads mainly through the respiratory tract (Tai et al., 2020). It affects type II alveolar (AT2) cells through interaction with the cell surface angiotensin-converting enzyme 2 (ACE2) via its spike protein (Wan et al., 2020; Xu et al., 2020; Zhao et al., 2020). This explains the development of acute respiratory syndrome in COVID-19 patients (Wan et al., 2020; Zheng et al., 2020). This also suggests that the spike protein-mediated SARS-CoV-2 attachment, fusion, and entry into the cells may be an interesting target for the development of antibodies and entry inhibitors, as a means to reduce the risks or attenuate the progression of the infection (Singh et al., 2020). Therefore, this study developed an EIS-based biosensing platform consisting of a recombinant ACE2 protein-coated palladium nano-thin-film (ACE2-Pd-NTF) electrode as the core sensing element to detect alterations that may occur in the binding of SARS-CoV-2 spike protein (S-protein) to ACE2 when exposed to modulating molecules (Scheme 1), as an efficient tool to identify potential pharmacological inhibitors against SARS-CoV-2-ACE2

binding.

The potential of the current EIS-based biosensing platform for identifying pharmacological inhibitors for SARS-CoV-2-ACE2 binding was assessed through the screening of a panel of the U.S. Food and Drug Administration (FDA)-approved peptide analogs predicted to promote hydrogen bonding interactions with ACE2 via computational structural superimposition analysis. In this study, we report the screening results of selected peptide analogs that exhibited inhibition against SARS-CoV-2-ACE2 binding at both the molecular and cellular levels. A few peptide analogs exhibited positive modulation of SARS-CoV-2-ACE2 binding. These findings demonstrate the capability of the developed biosensing platform to screen modulators of SARS-CoV-2-ACE2 binding at the molecular level.

2. Materials and methods

2.1. Computational structural modeling-receptor superimposition analysis

The crystal structures of ACE2 (1R4L) and angiotensin-converting enzyme (ACE) (1UZE, 2X94, 1O86, and 2X92) were obtained from the Protein Data Bank ([rcsb.org](https://www.rcsb.org)) (Berman et al., 2000) and superimposed to assess the structural similarities. To select the candidates for the biosensing-based SARS-CoV-2-ACE2 binding inhibitor screening experiments, the chemical structure of a panel of peptide analogs known to inhibit ACE (e.g., lisinopril, enalaprilat, perindoprilat, and ramiprilat, PDB ID: 1O86, 1UZE, 2X94 and 2X92, respectively) were superimposed virtually onto MLN-4760 (ACE2 inhibitor)-ACE2 complex (PDB ID: 1R4L) and examined *via* superimposition function in Discovery Studio Visualizer to generate their respective interaction diagrams.

2.2. Recombinant expression and characterization of ACE2 and SARS-CoV-2 S-protein

The recombinant ACE2 and SARS-CoV-2 S-protein receptor-binding domain (referred to as S-protein) were expressed through the *Escherichia coli* system (Chang et al., 2019a). Gene sequences for ACE2 and S-protein were obtained from SWISS-MODEL (Waterhouse et al., 2018) and were synthesized using the chemical synthesis method by Genomics Co. (Taipei, Taiwan). The synthesized ACE2 and S-protein gene fragments were then sub-cloned into pUC expression vectors (Fig. S1), and the resulting vectors were transformed into the XLI-Blue strand *E. coli* host (Chang et al., 2019a). To overexpress the recombinant ACE2 and S-protein, the refreshed host in 250 mL Luria-Bertani (LB) medium was induced with 0.5 mM isopropyl β-D-thiogalactopyranoside (IPTG) at 37 °C for 18 h. Recombinant ACE2 and S-protein were isolated from the bacterial inclusion body and refolded with the quasi-static over-critical folding process. Briefly, denatured ACE2 or S-protein from the inclusion body was dissolved in a denature buffer (Chang et al., 2002). The denatured proteins were then refolded by reducing the concentration of denaturant and salts in the protein solution and gradually adjusting the solution pH from 12 to 8.8. The ACE2 and S-proteins were expected to refold after a series of buffer changes. Upon completion of the protein refolding, western blotting (using anti-ACE2 and anti-S-protein antibodies) was performed to confirm the identity and purity of the

expressed ACE2 and S-protein (Xu et al., 2015). The concentrations of ACE2 and S-protein were determined using ultraviolet–visible (UV–vis) spectroscopy at a wavelength of 280 nm.

2.3. nCoV-S pseudovirus

The nCoV-S Luc pseudovirus was obtained from the National RNAi Core Facility at Academia Sinica, Taiwan by using, pCMVdeltaR8.91 and pcDNA3.1 to express S-proteins on the surface of the pseudovirus. The entry of pseudovirus can be identified by the luminescence emitted from the luciferase encoded in the transfer vector pLAS2w.FLuc.Ppuro.

2.4. ACE2 and S-protein dot blot binding assay

A dot blot binding assay was performed to assess the affinity of the synthesized recombinant S-protein to recombinant ACE2. The PVDF membrane was activated using 100% ethanol for 1 min before the deposition and drying of ACE2 protein (0.2 mg/mL) onto the membrane at the center of the grid (3–4 mm in diameter). The membrane was then incubated in a blocking solution (5% skim milk in TBS-T) for 1 h, followed by incubation with alkaline phosphatase-conjugated S-protein (1.25–2500 pM) for 2 h at room temperature. The membrane was then washed three times with TBS-T for 5 min and incubated with NBT/BCIP reagent for 1–15 min. The density of the dark-colored dots developed on the membrane was quantified using the densitometry program (ImageJ, NCBI).

2.5. Design and characterization of electrochemical impedance spectroscopy (EIS)-based biosensor

The Palladium nano-thin film (Pd-NTF) electrode was fabricated according to a previously reported method (Chang et al., 2019a). Two granule layers of Pd were deposited on the PET substrate by a sputtering process to produce a Pd-NTF electrode. The crystalline structure of the Pd thin film was investigated using a low-temperature X-ray diffractometer (XRD) (D8, Bruker, Billerica, MA, USA). The scan range was from 20° to 60°, in increments of 0.05°/s. Thereafter, with a fixed small-angle incident X-ray beam at 1°, the XRD signal was analyzed via the Scherrer equation, as shown below:

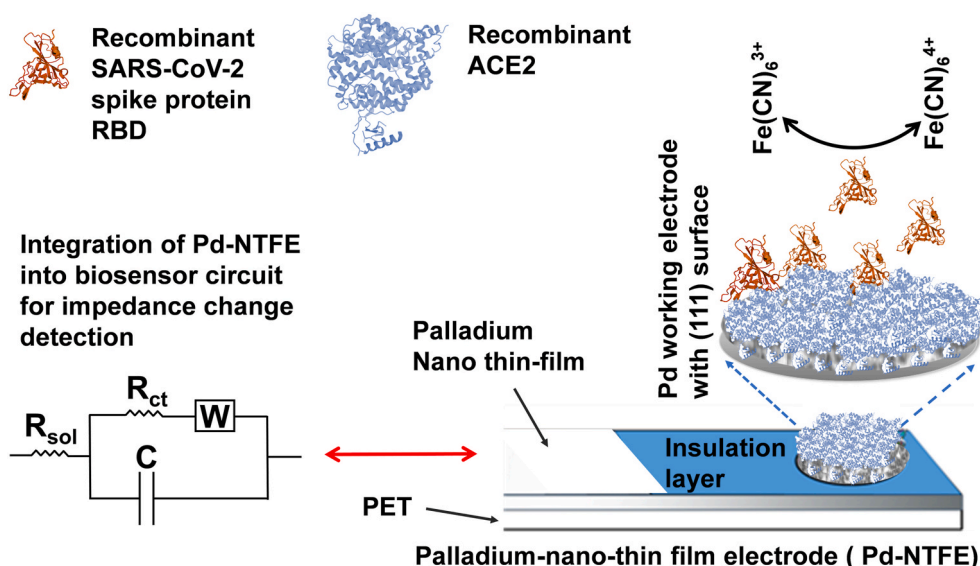
$$\tau = \frac{K\lambda}{\beta \cos\theta} \quad (1)$$

where, τ denotes the grain size, K the dimensionless shape factor (~ 0.89), λ the X-ray wavelength, β the full width at half maximum of the intensity (FWHM), and θ the Bragg angle. The wavelength of X-ray in this study was 1.54 Å.

To fabricate the biosensing electrode, 1 μ L of the recombinant ACE2 (0.8 mg/mL) was deposited onto the Pd-NTF electrode and incubated at room temperature for 20 min to form a functional ACE2 layer through the direct formation of Pd–S bonds between ACE2 and the active Pd surface (Chang et al., 2019a,b). The ACE2-coated Pd-NTF electrode was then rinsed with double distilled water to remove excess protein, followed by blocking with 1 μ L of 1-octadecanethiol (0.1 mM) at room temperature for 10–15 min. Subsequently, the ACE2-Pd-NTF electrode was coupled to the impedance spectroscopy device/amplifiers to form the complete ACE2-Pd-NTF biosensor-EIS setup. The Raman spectra of ACE2 immobilized on the Pd-NTF electrode were obtained using a custom-built micro-Raman system (Chang et al., 2019a). The Raman signal was analyzed using an ANDOR KYMERA-328i-A instrument with an ANDOR DR-05880 (Andor Tech. Ltd., Oxford Instruments, Belfast, UK). The prepared ACE-Pd-NTF electrode was also analyzed using impedance spectroscopy. The successful coating of ACE2 onto the Pd-NTF was determined by the increase of R_{ct} on Pd-NTF after the ACE2 coating. Subsequently, the ACE2-Pd-NTF biosensing electrode was coupled to the impedance spectroscopy device/amplifiers to form the complete ACE2-Pd-NTF biosensor-EIS setup.

2.6. Identification of SARS-CoV-2 – ACE2 binding modulators via EIS-based biosensing platform

In this study, we assessed the modulating effects of ACE2-interacting peptide analogs of the angiotensin-converting enzyme inhibitor (ACEi) class, such as enalapril, enalaprilat, lisinopril, captopril, perindopril, perindoprilat, ramipril, and ramiprilat, on S-protein-ACE2 interaction. The surface of ACE2-Pd-NTF electrode was pre-treated with 1 μ L of these ACEi (prepared in PBS at a concentration of 0.1–4 μ g/mL), as well as PBS (blank control) for 10 min at room temperature. The treated ACE2-Pd-NTF electrode was then gently rinsed with distilled water and drained dry prior to connecting to the EIS device for impedance measurement. The R_{ct} value obtained from the treated ACE2-Pd-NTF electrode was taken as the baseline R_{ct} . The treated ACE2-Pd-NTF electrode was then exposed to a series of PBS solutions containing ascending concentrations of S-protein (0.1–100 μ M, 2 μ L per electrode) for 10 min at room temperature, followed by EIS measurement. The net changes in R_{ct} value



Scheme 1. The EIS-based biosensing platform with ACE2-Pd-NTF electrode as biosensing probe against SARS-CoV-2's S-protein.

(ΔR_{ct}) were calculated by subtracting the baseline R_{ct} signals of ACE2-Pd-NTF electrode from that treated with PBS of S-protein. All ΔR_{ct} values were further normalized and expressed as the percentage of S-protein-ACE2 interaction by using the ΔR_{ct} values of the PBS-control group and the saturated S-protein-treated group as the 0% and 100% S-protein-ACE2 interaction, respectively (GraphPad Prism 8.3 software). A dose-response curve (S-protein concentration vs. ΔR_{ct}) was then plotted for the respective ACEi- and PBS-treated groups. The dose-response curves of the ACEi-treated groups were compared to those of the PBS-treated controls to assess the effect of the peptide analogue on the ACE2-S-protein interaction. To verify the binding selectivity of the S-protein to the ACE2-Pd-NTF electrode, the binding of the S-protein to the plain and non-ACE2 protein-coated Pd-NTF electrodes (in the absence and presence of selected model drugs, i.e., perindoprilat and lisinopril), were assessed. The binding of S-protein, albumin, and lysozyme to ACE2-Pd-NTF electrodes were also tested.

2.7. Cell culture and western blot analysis

OEC-M1 cells were cultured in RPMI 1640 medium supplemented with 10% fetal bovine serum (FBS), 100-unit penicillin, 100 μ g streptomycin, and 0.25 μ g fungizone (all from Gibco, Thermo Fisher, Waltham, MA, USA) per milliliter. The cells were seeded into a 6-well plate at a density of 3×10^5 cells/well for 18 h at 37 °C and 5% CO₂ before treatment. The expression of ACE2 in OEC-M1 cells in the absence or presence of selected peptide analogs (after 30 or 60 min of treatment at 20 μ M) was evaluated by western blotting. Briefly, the cells were lysed in lysis buffer (20 mM Tris-HCl pH 7.5, 150 mM NaCl, 2 mM EDTA, and 1% Triton X-100) to obtain crude extract. The proteins were subjected to 10% SDS-PAGE and transferred onto a PVDF membrane (Millipore, Burlington, MA, USA) in a wet transfer system (Bio-Rad, Hercules, CA, USA) for 120 min at 400 mA. The PVDF membrane was then incubated in blocking solution (5% milk powder in PBS containing 0.1% Tween 20), followed by probing with primary antibodies [rabbit anti-ACE2 (ab108252, 1/1000 dilution, Abcam, Cambridge, UK) and mouse anti- α -tubulin (GTX628802, 1/20,000 dilution, GeneTex, Irvine, CA, USA)]. Anti-mouse and anti-rabbit IgG-conjugated horseradish peroxidase antibodies (1:10,000) were used as secondary antibodies. Peroxidase activity was visualized using Enhanced Chemiluminescence kit (Millipore, Burlington, MA, USA). Chemiluminescence imaging was performed using a BioSpectrum Imaging System (UVP, USA), and densitometric analyses were performed using Alphamager 2200 software (ProteinSimple, Santa Clara, CA, USA).

2.8. Preparation of S-protein conjugated quantum dot (QD-S-protein)

A cadmium selenide core - zinc oxide shell (CdSe@ZnO) quantum dot (QD) (particle size \approx 2.5 nm, excitation and emission wavelengths at 400 and 525 nm, respectively), was a gift from Professor Dai-wen Pang of Nankai University, China (Liu et al., 2011). The QD-labeling of S-protein was done by adding carboxyl-modified QD to the S-protein at a molar ratio of 1:5 in 500 μ L of deionized water containing 0.1M 1-ethyl-3-(3-dimethylaminopropyl) carbodiimide (EDC, Merck KGaA, St. Louis, MI, USA) (East et al., 2011). The reaction mixture was then incubated for 12 h at 4 °C on a rotating wheel in the dark. Thereafter, the reaction mixture was dialyzed in a dialysis tube with 3 kDa molecular weight cut off against 50 mM Tris-HCl buffer pH 7.5 for three rounds (10 h/round) to remove excess EDC from the mixture. Estimation of the QD-labeled S-protein concentration in the dialyzed product was then performed via UV spectroscopy (at a wavelength of 280 nm with the S-protein extinction coefficient (ϵ) of 45240 M⁻¹ cm⁻¹). The mechanism of QD labeling of the S-protein is illustrated in Fig. S2.

2.9. Confocal microscopy for S-protein uptake by oral squamous cell carcinoma (OEC-M1) cells

To detect S-protein uptake by OEC-M1 cells, the cells were seeded on glass cover slides in 24-well plates and left to attach overnight. The cells were then treated with 800 nM purified QD-S-protein for 30, 60, and 120 min. After removing QD-S-protein from the medium and washing thrice with PBS, the cells were fixed with 4% paraformaldehyde. Fluorescent and cellular morphology images were captured with a digital camera and a charge-coupled device image sensor with a differential interference contrast channel (FluoView FV1000, Olympus, Tokyo, Japan). High-resolution images were scanned from bottom to top (z-sections) to evaluate QD-S-protein *in vitro* binding.

2.10. In vitro SARS-CoV-2 infectivity

ACE2-expressing OEC-M1 cells (2×10^5 cells) were pretreated with 20 μ M of enalapril, enalaprilat, lisinopril, captopril, perindopril, or ramipril for 30 min, followed by exposing to 1 MOI (multiplicity of infection) of SARS-CoV-2/human/TWN/CGMH-CGU-01/2020 for 60 min in the presence of the respective peptide analogs (20 μ M). A blank control was also included, in which the cells received similar treatment except for the peptide analogs in the cell culture media. After incubation, all cells were washed with PBS and incubated at 37 °C for another 24 h. At the end of the 24-h incubation, cell culture media were collected, and SARS-CoV-2 RNA was extracted from the media using LabTurbo Viral Mini Kit, with LabTurbo 48 Compact System (LabTurbo, Taipei, Taiwan). cDNA was synthesized using the MMLV Reverse Transcription Kit (Protech, Taipei, Taiwan). The primers and probes were targeted to the viral E gene of SARS-CoV-2. The primer and probe sequences for the E gene were as follows:

Primer: forward 5'- ACAGGTACGTTAATAGTTAATAGCGT- 3'; reverse 5'-ATATTGCAGCAGTACGCACACA-3'.

Probe: 5'-FAM- AACTAGCCATCCTTACTGCGCTTCG-BBQ-3'.

The Roche LightCycler®480 System (Roche, Basel, Switzerland) and 2 \times qPCR BIO Probe Blue Mix Lo-ROX (Kapa Biosystems, Wilmington, MA, USA) were used for quantitative detection of nucleic acids.

3. Results

3.1. EIS-based biosensor design and characterization

In this study, we developed an EIS-based biosensing platform (Chang et al., 2019a, 2019b) to identify potential pharmacological inhibitors from the selected FDA-approved ACE/ACE2-interacting peptide analogs to the ACE2-SAR-CoV-2's S-protein interaction.

First, a unique Stranski-Krastanov-like palladium thin film (Pd-NTF) electrode was fabricated through the epitaxial sputtering of two or three layers of Pd nanoparticles onto a polyethylene terephthalate (PET) substrate according to previous methods (Chang et al., 2019a, 2019b). The fabricated Pd-NTF electrode was found harboring a retainable Pd surface with specifically coordinated Pd (111) and Pd (200) nanocrystalline structures (granule size respectively at \sim 3.81 nm and \sim 6.09 nm, estimated based on the Scherrer equation) that favors the conjugation of biomolecules.

To protect the electrode surface from reacting with the environmental elements, a thin layer of indium tin oxide (ITO) was used to cover the surface. Immediately before bio-conjugation, the ITO coating was removed via oxalate acid etching. The XRD analysis indicated that the ITO coating and removal processes did not change the Pd surface structure or the bio-conjugation efficiency (Chang et al., 2019b) (Fig. 1A). Subsequently, the fabricated Pd-NTF electrode was exposed to the recombinant ACE2 protein (0.8 mg/mL) to allow its rapid immobilization (within 20 min) on the electrode surface to form the ACE2-coated palladium nano-thin-film (ACE2-Pd-NTF) electrode (Fig. 1B). Prior to this, recombinant ACE2 and SARS-CoV-2 S-protein

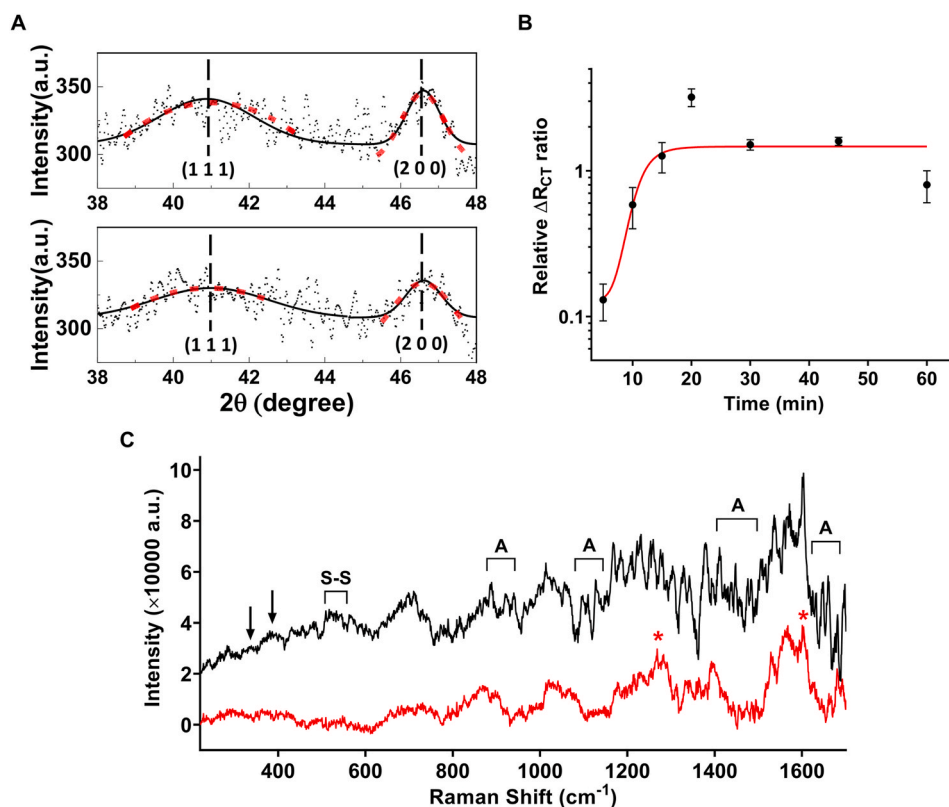


Fig. 1. Characterization of ACE2-Pd-NTF electrode. (A) The XRD spectra of Pd-NTF covered with ITO (upper panel) and after removal of ITO (lower panel). The black lines denoted the noise reduction XRD spectra. The red dash lines denoted the Gaussian fitting peaks of Pd (111) or Pd (200). (B) Time-dependent ACE2 bio-conjugation. (C) Raman spectra of ACE2 on Pd-NTF (Black line) and Pd-NTF only (Red line). The black arrows denoted the vibration mode of Pd-S bonding (Chang et al., 2019a; Merkle et al., 1999). The red asterisks denote the typical PET signal, and S-S denotes the vibration mode of protein disulfide bonds. The A regions represent the protein specific signals. (For interpretation of the references to color in this figure legend, the reader is referred to the Web version of this article.)

were expressed and confirmed by Western blots. The binding of S-protein to ACE2 was verified by dot blot assay (Fig. S3).

Raman spectroscopy analysis (Fig. 1C) indicated that ACE2 was immobilized on the Pd-NTF surface via Pd-S linkage with a “Braggite-like” Raman shift from 326 to 392 cm^{-1} (Chang et al., 2019a; Chang et al., 2019b; Merkle et al., 1999). The Raman shifts from 500 to 1700 cm^{-1} contained signals for the ACE2 protein and the PET substrate (Fig. 1C) (Lippert et al., 1976; Stewart and Fredericks 1999; Tuma 2005; Zhu et al., 2015). These results indicated that ACE2 could bind to the Pd-NTF surface within 20 min with only 0.8 μg . The ultrasensitive detection of Raman spectroscopy signals at low sample amounts in the current analysis may be attributed to the induction of a local surface plasmon resonance (LSPR) phenomenon and an enhanced surface electric field by the unique Pd metal nanostructure on the surface of the biosensing electrode (Xu et al., 2015). Furthermore, the enhanced surface electric field generated may reduce the surface impedance of the electrode, thus elevating the sensitivity of signal detection in electrochemical impedance spectroscopy (EIS).

The binding of the viral S-protein or virus to the immobilized ACE2 and the interfering effects of pharmacological inhibitors were detected by monitoring the changes in the electrical impedance at the interface of the solution and S-protein/virus – ACE2-Pd-NTF electrode. Such electrical impedance can be determined by applying a small sinusoidal voltage at different frequencies to the S-protein/virus-ACE2-Pd-NTF electrode, followed by measuring the resulting sinusoidal current responses. Moreover, impedance was calculated based on the current-voltage ratio via an effective equivalent Randel’s model derived from the model proposed by Ramanavicius et al. (2010), whereby the charge transfer resistance (R_{ct}) represented the impedance from the ACE2-spike binding and was equivalent to the effective CPE in Ramanavicius’ model (Chang et al., 2019a, 2019b; Cheng et al., 2011; Li et al., 2013; Ramanavicius et al., 2010). Further technical details of this EIS-based biosensing platform were provided in the supplementary section.

The capability of this EIS-biosensing setup to detect the binding of SARS-CoV-2 to ACE2 was first demonstrated through the successful

binding of the nCoV-S-Luc pseudovirus (a SARS-CoV-2 pseudovirus obtained from the National RNAi Core Facility at Academia Sinica, Taiwan) to the ACE2-Pd-NTF electrode in a dose-dependent manner (Fig. 2A and Fig. S4). Although the nCoV-S-Luc pseudovirus is an optimal substitute for the SARS-CoV-2 virus for a variety of physiological and cellular studies, it is not suitable for the evaluation of pharmacological inhibitor effects in this study because its stock concentration can only be estimated by the relative infection unit (RIU). Therefore, a recombinant viral spike protein receptor-binding-domain fragment (herein referred to as S-protein) of SARS-CoV-2 virus was adopted as a model system to investigate the effect of pharmacological inhibitors on the interaction between S-protein and ACE2. Fig. 2B shows a dose-response curve (with effective S-protein concentration to trigger 50% S-protein-ACE2 binding signals, $EC_{50-S} @ \text{baseline} = 1.74 \pm 0.31 \mu\text{M}$) that reflects the dose-dependent interaction of recombinant viral S-protein to the ACE2-Pd-NTF electrode.

3.2. Selection of SARS-CoV-2-ACE2 binding inhibitor candidates via computational structural superimposition analysis

Through a computational structural superimposition analysis, the 3-dimensional structures of ACE and ACE2 complexes were well aligned with each other (Fig. 3). This was in line with previous reports that ACE and ACE2 share 40% sequence identity and >60% sequence similarity (Chappel and Ferrario 2006; Donoghue et al., 2000; Tipnis et al., 2000). Based on these findings, we performed superimposition analysis on a panel of peptide analogs known to inhibit ACE to assess their possible interaction with ACE2.

Through the superimposition analysis, several peptide analogs of the pharmacological ACE inhibitor (ACEi) class that possess a (2-oxoethyl) glycine moiety (Fig. 3 and Fig. S5) resembled that of the classical ACE2 inhibitor MLN-4760 (Towler et al., 2004b) and its analogs, such as lisinopril, enalaprilat, perindoprilat, and ramiprilat, were found to promote important interactions with the key amino acid residues in the active site of ACE2 via hydrogen bonding (Akif et al., 2010; Natesh et al.,

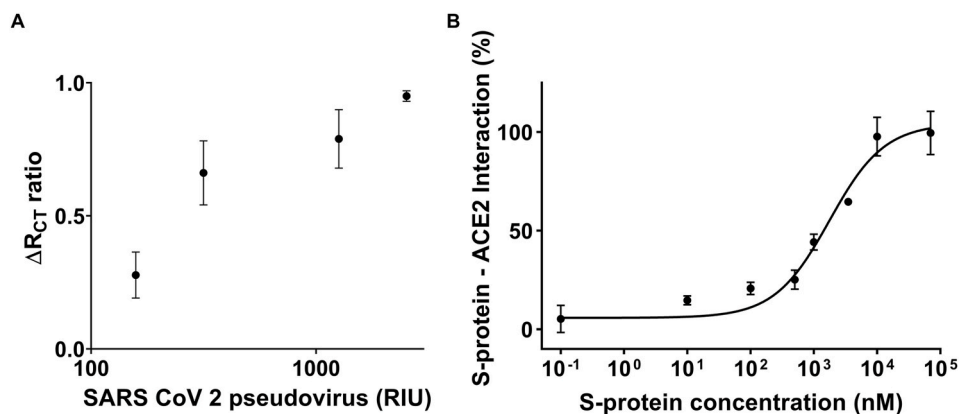


Fig. 2. Electrochemical impedance sensing correlates with SARS-CoV-2 pseudovirus or S-protein binding. (A) Relative impedance change ratios (ΔR_{CT} ratio) in response to the ascending concentrations of SARS-CoV-2 pseudovirus. (B) Dose-response curve of the S-protein interaction with the ACE2 (EC_{50-S} @ baseline = $1.74 \pm 0.31 \mu$ M, generated via the biosensing platform). Error bars indicate SD.

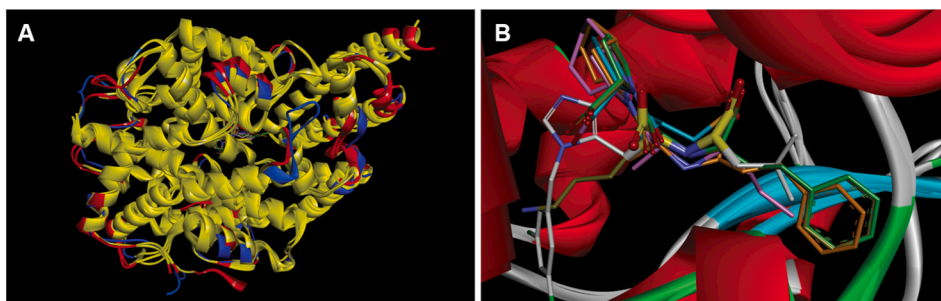


Fig. 3. Molecular modeling and small molecule docking of ACE2. (A) Superimposition of ACE2/MLN-4760 binary complex and ACE/ACEi complexes. The overlapping regions colored in yellow [main-chain root-mean-square deviation (RMSD) values for aligned residues are $\leq 2.0 \text{ \AA}$ with 1R4L as a reference] while the non-overlapping regions are colored in red for ACE (main-chain RMSD values for aligned residues are $> 2.0 \text{ \AA}$ with 1R4L as reference) and blue for the related ACE2 regions. (B) Superimposition of MLN-4760 (white), enalaprilat (green), perindoprilat (pink), lisinopril (gold), and ramiprilat (orange) in ACEs binding pocket. The carbon atoms of acetone-glycine moiety are colored in yellow. (For interpretation of the references to color in this figure legend, the reader is referred to the Web version of this article.)

interpretation of the references to color in this figure legend, the reader is referred to the Web version of this article.)

2003, 2004; Towler et al., 2004a) (Fig. 3B and Fig. S5). Hence, these compounds were selected as candidates for the subsequent screening of SARS-CoV-2-ACE2 binding inhibitors using the developed biosensing platform.

3.3. Identification of SARS-CoV-2 – ACE2 binding modulators via EIS-based biosensing platform

To further explore the potential of ACEi in modulating the interaction of S-protein and ACE2, the ACE2-Pd-NTF electrodes were exposed to the shortlisted ACEi, which included lisinopril, captopril, enalaprilat, perindoprilat, ramiprilat, and the corresponding prodrugs, enalapril, perindopril, and ramipril. Thereafter, the electrodes were incubated with ascending concentrations of the S-protein. Changes in the electrode impedance were subsequently documented and analyzed to reveal the presence and mode of modulation brought by ACEi to ACE2-S-protein binding.

Among the ACEi tested, perindopril, perindoprilat, ramipril, and ramiprilat were found to elicit a concentration-dependent suppression of the ACE2-S-protein interaction (Fig. 4). At 4 μ g/mL, perindopril and perindoprilat suppressed the ACE2-S-protein interaction by approximately 48% (E_{max-S} @ perindopril = $51.9 \pm 5.3\%$) and 67% (E_{max-S} @ perindoprilat = $33.0 \pm 3.7\%$), respectively (Fig. 4A, B). In comparison, the E_{max-S} @ baseline was $99.5 \pm 11.0\%$ ($p < 0.01$) for the baseline control. Similarly, ramipril at 4 μ g/mL suppressed the binding of S-protein to ACE2 by approximately 42% (E_{max-S} @ ramipril = $57.1\% \pm 11.4\%$) (Fig. 4C). Ramiprilat exhibited 30% stronger inhibition than ramipril (72% suppression of the binding of S-protein to ACE2 with E_{max-S} @ ramiprilat = $27.6 \pm 7.5\%$) (Fig. 4C, D). Both active metabolites of perindopril and ramipril exhibited stronger suppressive effects than the

parent compounds. These findings indicate correlations of the suppressive activities to the metabolic alteration of the inhibitors' chemical structures. Moreover, it suggests the potential of perindopril and ramipril and their metabolites as pharmacological inhibitors of the SARS-CoV-2 – ACE2 binding. The ability of the developed EIS-based biosensing platform to identify inhibitors against ACE2-S-protein binding has been clearly demonstrated for the first time in this study.

It should be noted that not all ACEi can exhibit inhibitory action against S-protein – ACE2 binding. In this study, the EIS-based biosensing platform surprisingly identified the positive modulators of the S-protein – ACE2 binding from among the peptide analogs tested. For example, enalapril, its active metabolite enalaprilat, and lisinopril were found to enhance ACE2-S-protein binding in a dose-dependent manner (Fig. 4E–G). At 4 μ g/mL, enalapril, enalaprilat and lisinopril increased S-protein binding affinity to ACE2 by 25- (EC_{50} = $0.07 \pm 0.01 \mu$ M), 174- ($0.01 \pm 0.003 \mu$ M) and 67-fold ($0.03 \pm 0.005 \mu$ M), respectively, compared to the baseline control (EC_{50-S} @ baseline = $1.74 \pm 0.31 \mu$ M) ($p < 0.001$). However, captopril did not cause a significant alteration in the ACE2-S-protein interaction compared to the control. For example, at 4 μ g/mL captopril, the EC_{50} value (EC_{50-S} @ captopril = $5.1 \pm 2.62 \mu$ M) was not significantly different to that of the control (Fig. 4H).

In assessing the binding selectivity of the S-protein to the Pd-NTF electrodes, S-protein was found to bind to the plain Pd-NTF electrodes and to the lysozyme-coated Pd-NTF electrodes only at high S-protein concentration, and the presence of perindoprilat and lisinopril did not change the S-protein's binding patterns to these electrodes significantly (Fig. S6). Furthermore, a concentration-dependent elevation in S-protein-ACE2 binding signals was seen when ACE2-Pd-NTF electrode was incubated in ascending concentrations of S-protein, but not in lysozyme and albumin at equivalent concentration range (Fig. S7). These findings

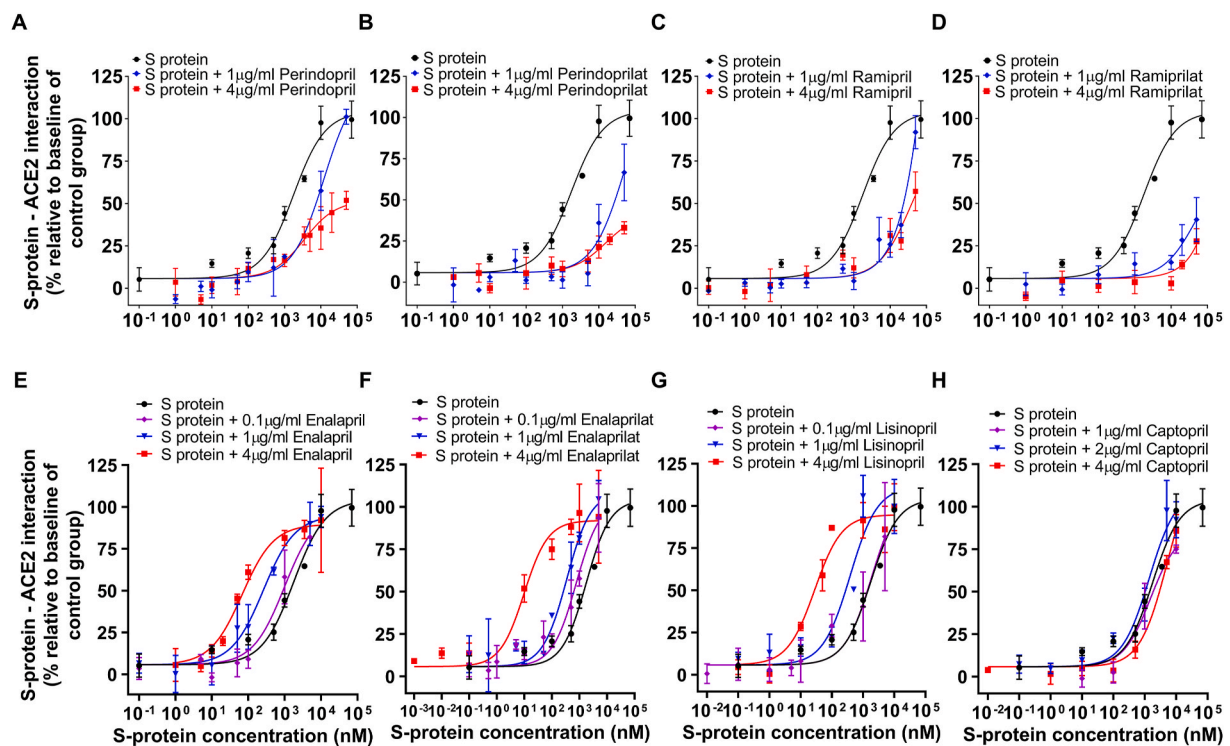


Fig. 4. Elucidation of the effects of the selected ACEi to ACE2-S-protein binding through the use of an EIS-based biosensing platform. The interaction of S-protein and ACE2 in the presence of 0 µg/mL, 1 µg/mL, and 4 µg/mL of (A) perindopril, (B) perindoprilat, (C) ramipril, (D) ramiprilat; and 0 µg/mL, 0.1 µg/mL, 1 µg/mL and 4 µg/mL of (E) enalapril, (F) enalaprilat (G) lisinopril and (H) captopril were measured and analyzed on the EIS-based biosensing platform. Error bars indicate SD.

suggested selective interaction of S-protein with ACE2 protein-coated Pd-NTF electrodes.

3.4. *In vitro* SARS-CoV-2 infectivity study

The modulation of ACE2-S-protein binding by the selected ACEi was subsequently verified with an *in vitro* SARS-CoV-2 infectivity study (Fig. 5). In this study, ACE2-expressing human oral cavity squamous cell carcinoma cells (OEC-M1) pretreated with the selected ACEi (20 µM, 30 min) and saline (blank control) were exposed to 1 multiplicity of infection (MOI) of SARS-CoV-2 (SARS-CoV-2/human/TWN/CGMH-CGU-01/2020). The viral envelope protein gene (E gene) RNA in the cell culture media was quantified 24 h post virus incubation to assess infectivity. Before the study, the expression of ACE2 in OEC-M1 cells was confirmed via Western blot analysis, and ACE2 expression was not affected by treatment with the selected peptide analogs (Fig. 5A). The ability of the expressed-ACE2 in interacting with the SARS-CoV-2 was also demonstrated indirectly through the successful uptake of a quantum dot-labeled S-protein (QD-S-protein) into the OEC-M1 cells (Fig. 5B and S8), presumably through the ACE2 receptor.

Upon treatment with ramipril and ramiprilat, E gene RNA copies in the culture media of OEC-M1 cells were reduced by 39.3% and 36.4%, respectively (both $p < 0.05$ vs. blank control). In contrast, E gene RNA copies reduced by approximately 18.8% and 20.1% with perindopril and perindoprilat treatments ($p < 0.05$ for perindoprilat vs. blank control) (Fig. 5C). However, E gene RNA copies were increased by 93.7%, 44.4%, and 54.2% relative to the blank control ($p < 0.05$) in the media from cells treated with enalapril, enalaprilat, and lisinopril, respectively. Interestingly, the E gene RNA copy for the captopril-treated group was elevated by 34.5%, suggesting possible positive modulation of SARS-CoV-2 – ACE2 binding by captopril *in vitro*. These findings confirmed the results of the EIS-based biosensing study and demonstrated the potential use of the developed EIS-based biosensing platform for rapid screening of inhibitors for SARS-CoV-2 – ACE2 binding.

4. Discussion

In this study, we have successfully developed an EIS-based biosensing platform that is capable of identifying both positive and negative modulators of the SARS-CoV-2's S-protein-ACE2 binding. This sensor platform offers sensitive and rapid detection of the binding of modulators to ACE2 in a small sample volume (1 µL). With this detection system the binding of as little as 4 pg or 0.1 µg/mL modulator could be detected. The elevated detection sensitivity of this thin film biosensing platform may be correlated to the enhanced local surface plasmon resonance and electric field (for better Raman signals and EIS detection) on the biosensing electrode by its multi-layered Pd surface nanostructure (Hong et al., 2016; Li et al., 2018). Such a unique Pd nanogranule coating also enabled direct immobilization of the recombinant ACE2 to the probes within 20 min, with which the fabrication of the biosensing electrode was greatly accelerated and simplified.

Through the EIS-based biosensing experiment, we showed that selected peptide analogs of the pharmacological ACEi class may modulate the binding of SARS-CoV-2's S-protein to the ACE2 receptor differentially in a dose-dependent manner, depending on their chemical structures. ACEi is a class of peptide analogs that competitively inhibit angiotensin converting enzyme I (ACE) to suppress the formation of angiotensin II, and consequently decreases the activation of angiotensin II type 1 (AT1) receptor and related pharmacological events, such as vasoconstriction, sodium and water retention, and sympathetic activation (Messerli et al., 2018). At present, these compounds are among the commonly prescribed medications for the management of cardiovascular diseases and hypertension (Messerli et al., 2018; Ponikowski et al., 2016; Sommerstein et al., 2020).

From the EIS data, ACEi that possess a bulky group of the rigid fused ring in their structure, such as the cyclopenta[b]pyrrole-2-carboxylic acid moiety in ramipril/ramiprilat (Fig. 6a) and the 1*H*-indole-2-carboxylic acid moiety in perindopril/perindoprilat (Fig. 6b), may antagonize ACE2-S-protein binding (Fig. 4A–D); ACEi without such bulky

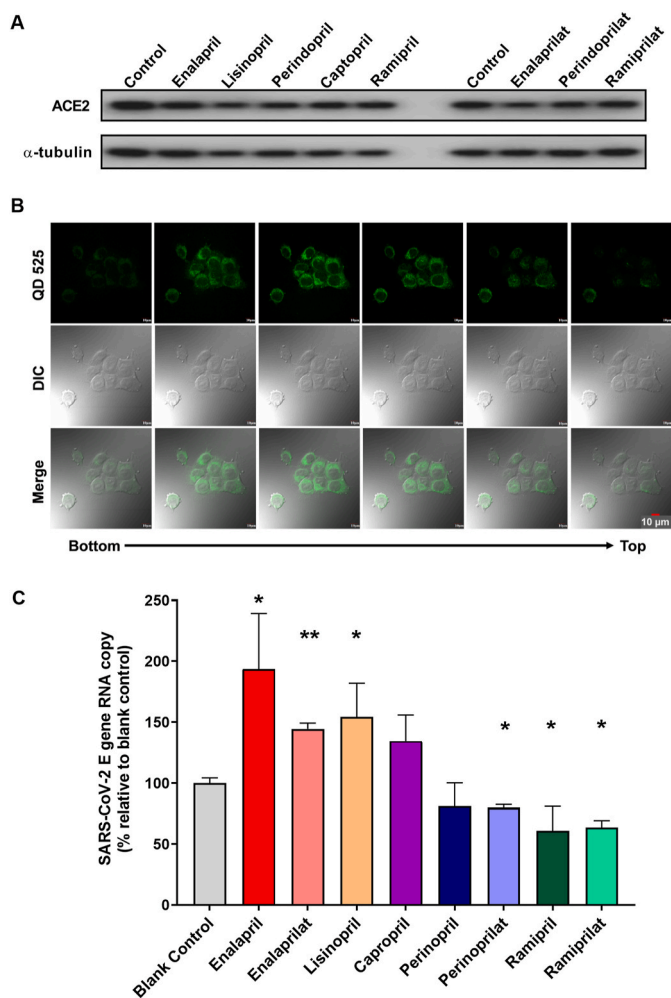


Fig. 5. Differential effect of selected ACEi on SARS-CoV-2 uptake *in vitro*. (A) Expression of ACE2 by the OEC-M1 in the absence or presence of various selected peptide analogs (30 and 60 min pre-treatment at 20 μ M respectively). (B) Z-stack confocal microscopic images (1 μ m slicing) of OEC-M1 cells after treated with QD-S-protein for 30 min. (C) Alterations in the viral E gene RNA copy number in OEC-M1 culture pretreated with selected ACEi (relative to blank control, * $p < 0.05$, unpaired *t*-test). Error bars are in SD.

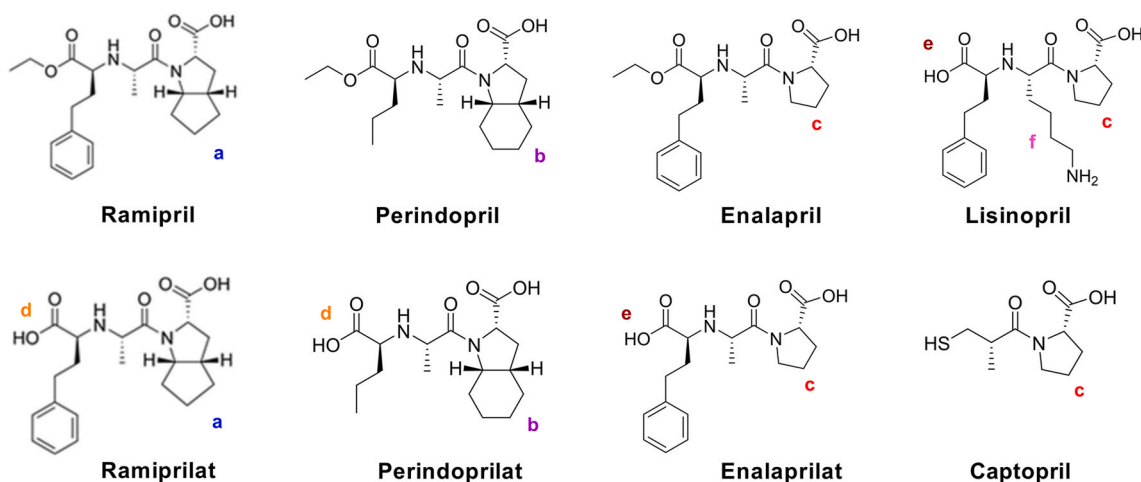


Fig. 6. Chemical structures of ACEi screened via the EIS-based biosensing platform. The “a” denoted the cyclopenta[b]pyrrole-2-carboxylic acid moiety; “b” denoted the 1H-indole-2-carboxylic acid moiety; “c” denoted the pyrrole-2-carboxylic acid moiety; “d” denoted glycine moiety; “e” denoted the glycine-carboxyl terminal and “f” denoted the C₄H₈-NH₂ side chain at the L-lysyl moiety.

group, such as enalapril/enalaprilat and lisinopril (Fig. 6c), may positively modulate the ACE2-S-protein binding (Fig. 4E–G). The antagonizing effect of ramipril and perindoprilat (Figs. 6d and 4B, D) and the positive modulating effects of enalaprilat and lisinopril (Fig. 6e) may be further enhanced by their carboxyl-terminal at the glycine moiety. In contrast, an n-butyl amine (C₄H₈-NH₂) side chain at the L-lysyl moiety of lisinopril (Fig. 6f) may weaken its positive modulatory effect on ACE2-S-protein binding.

The observed differential modulation effects of the selected ACEi were further confirmed through an *in vitro* SARS-CoV-2 infectivity study. As shown in Fig. 5C, the SARS-CoV-2 infectivity was suppressed upon exposure to ramipril, ramiprilat, perindopril, and perindoprilat, but; however, it was enhanced upon cell exposure to enalapril, enalaprilat, and lisinopril, as reflected by the changes in the viral E gene RNA copies in the media. These findings demonstrated the potential use of the developed EIS-based biosensing platform for rapid screening of modulators for SARS-CoV-2 – ACE2 binding.

Furthermore, captopril, which had a neutral effect on ACE2-S-protein binding in the EIS-biosensing experiment (Fig. 4H), tended to enhance the SARS-CoV-2 infectivity (Fig. 5C). The absence of ACE2-S-protein binding modulation by captopril in the biosensing experiment is most likely due to its chelation (via its sulfhydryl group) of the Fe²⁺ ions of the electrolyte (K₂Fe(CN)₆), making it unavailable for interaction with ACE2 on the electrode. Nevertheless, further studies are required to confirm the actual effects of captopril on SARS-CoV-2 infectivity, as the increase in the E gene RNA expression induced by captopril was found to be statistically insignificant in this experiment.

The findings on the attenuation of the ACE2-S-protein binding and SARS-CoV-2 infectivity by ramipril, ramiprilat, perindopril, and perindoprilat may suggest a direction in the development of molecules with similar bulky group of rigid fused ring structures (e.g., quinapril, benazepril, trandolapril, cilazapril, and moexipril) but devoid of the pharmacological effects of these compounds as adjunctive agents for the treatment of SARS-CoV-2 infection. In addition, the positive modulatory effects of lisinopril, enalapril, and enalaprilat on ACE2-S-protein binding and SARS-CoV-2 infectivity were unexpected and could be of clinical importance, as it may suggest an increased risk for SARS-CoV-2 infection in ACE2-expressing cells of patients who are on these medications.

To date, several preliminary clinical/meta-analysis studies have suggested that there is no significant association between ACEi use and the risk, severity, and mortality of COVID-19 (Fosbøl et al., 2020; Ghosal et al., 2020; Mehta et al., 2020; Reynolds et al., 2020). One study also suggested that the use of ACEi may reduce the mortality of COVID-19 patients compared to those not receiving these drugs (Ghosal et al.,

2020). However, many of these studies were found to perform their analysis without taking into consideration the type of ACEi administered (some included angiotensin receptor blockers in the analysis) (Fosbøl et al., 2020; Ghosal et al., 2020; Mehta et al., 2020; Reynolds et al., 2020). This study suggests that not all ACEi are equal and that different ACEi may impose different modes of modulation on SARS-CoV-2 cell uptake and infectivity. Therefore, epitomizing clinical data of COVID-19 patients who are on different types of ACEi may complicate the analysis and affect the accuracy of the outcome. Thus, a careful coupling of the patients' ACEi prescription records to their clinical history of COVID-19 may be critical for ascertaining SARS-CoV-2 infection risk and prognosis.

5. Conclusions

In this study, a sensitive EIS-based biosensor was developed to screen modulators of SARS-CoV-2 S-protein-ACE2 interaction. A few potential pharmacological leads, such as ramipril and perindopril, and their active metabolites ramiprilat and perindoprilat, that suppress SARS-CoV-2-ACE2 binding, were successfully identified. However, their therapeutic potential in attenuating the progression of infection requires further investigation. This study offers an alternative approach for the rapid screening of existing therapeutic drugs in drug-repurposing efforts to curb the COVID-19 pandemic. This study also provides updated data that support the use of electrochemical biosensing platforms as a simple, reliable, and rapid approach for the screening of potential inhibitors and modulators of pharmacological ligand-receptor interactions. Such an approach is yet to be fully explored at present. However, it has good potential for becoming a mainstream approach for efficient, time-saving, and cost-effective drug discovery and repurposing in the future (Kilic et al., 2018b). In addition, this report also suggests a new insight on how ACEi of different molecular structures may impose paradoxical modulation on the S-protein-ACE2 binding, which affects the SARS-CoV-2 infection risks and prognosis. However, the current findings are mainly *in vitro*, and further *in vivo* and clinical investigations are necessary to confirm the potential risks associated with the use of some ACEi in COVID-19 patients.

CRedit authorship contribution statement

Lik-Voon Kiew: Conceptualization, Methodology, Validation, Investigation, Formal analysis, Data curation, Writing – original draft, Visualization, Project administration. **Chia-Yu Chang:** Methodology, Validation, Investigation, Formal analysis, Data curation, Writing – original draft, Visualization, Project administration. **Sheng-Yu Huang:** Methodology, Validation, Investigation, Formal analysis, Data curation, Writing – original draft, Visualization. **Pei-Wen Wang:** Methodology, Validation, Investigation, Formal analysis, Data curation, Writing – original draft, Visualization. **Choon-Han Heh:** Methodology, Software, Investigation, Formal analysis, Data curation, Writing – original draft, Visualization. **Chung-Te Liu:** Investigation, Formal analysis. **Chia-Hsin Cheng:** Investigation, Formal analysis. **Yi-Xiang Lu:** Investigation, Formal analysis. **Yen-Chen Chen:** Investigation, Formal analysis. **Yi-Xuan Huang:** Investigation, Formal analysis. **Sheng-Yun Chang:** Investigation, Formal analysis. **Huei-Yu Tsai:** Investigation, Formal analysis. **Yu-An Kung:** Investigation, Formal analysis. **Peng-Nien Huang:** Investigation, Formal analysis. **Ming-Hua Hsu:** Methodology, Validation, Investigation, Formal analysis, Writing – review & editing, Visualization, Project administration. **Bey-Fen Leo:** Formal analysis, Writing – review & editing, Visualization. **Yiing-Yee Foo:** Formal analysis, Writing – review & editing, Visualization. **Chien-Hao Su:** Investigation, Formal analysis. **Kuo-Chen Hsu:** Investigation, Formal analysis. **Po-Hsun Huang:** Conceptualization, Formal analysis, Writing – review & editing. **Chirk-Jenn Ng:** Formal analysis, Writing – review & editing. **Adeeba Kamarulzaman:** Formal analysis, Writing – review & editing. **Chiun-Jye Yuan:** Formal analysis, Writing – review & editing,

Visualization. **Dar-Bin Shieh:** Conceptualization, Methodology, Formal analysis, Resources, Data curation, Writing – review & editing, Project administration, Funding acquisition. **Shin-Ru Shih:** Conceptualization, Methodology, Formal analysis, Resources, Data curation, Writing – review & editing, Project administration, Funding acquisition. **Lip-Yong Chung:** Conceptualization, Formal analysis, Writing – review & editing, Project administration. **Chia-Ching Chang:** Conceptualization, Validation, Methodology, Investigation, Formal analysis, Resources, Data curation, Writing – review & editing, Visualization, Supervision, Funding acquisition.

Declaration of competing interest

The authors declare that they have no known competing financial interests or personal relationships that could have appeared to influence the work reported in this paper.

Acknowledgements

We thank the National RNAi Core Facility at Academia Sinica, Taiwan for providing the nCoV-S-Luc pseudovirus and related services; MSc. Yu-Cheng Lin, Department of Chemistry, National Changhua University of Education, for his contribution of chemicals preparation. This study is supported in part by the Ministry of Science and Technology (MOST), Taiwan (ROC) MOST 107-2112-M-009-016-MY3, MOST 108-2314-B-006-009-MY3, MOST 109-2327-B-010-005, MOST 109-2327-B-009-001, MOST 109-2327-B-182-002 and MOST 109-2927-I-009-003. This work is also supported by the Ministry of Education through the SPROUT Project and the Center for Intelligent Drug Systems and Smart Biodevices (IDS²B) of NYCU, Taiwan.

Appendix A. Supplementary data

Supplementary data to this article can be found online at <https://doi.org/10.1016/j.bios.2021.113213>.

References

- Akif, M., Georgiadis, D., Mahajan, A., Dive, V., Sturrock, E.D., Isaac, R.E., Acharya, K.R., 2010. *J. Mol. Biol.* 400 (3), 502–517.
- Berman, H.M., Westbrook, J., Feng, Z., Gilliland, G., Bhat, T.N., Weissig, H., Shindyalov, I.N., Bourne, P.E., 2000. *Nucleic Acids Res* 28 (1), 235–242.
- Chang, C.-C., Su, Y.-C., Cheng, M.-S., Kan, L.-S., 2002. *Phys. Rev. E* 66 (2), 021903.
- Chang, C.-Y., Huang, Y.-T., Chang, P.-C., Su, C.-H., Hsu, K.-C., Li, X., Wu, C.-H., Chang, C.-C., 2019a. *Inorg. Chem. Commun.* 107, 107461.
- Chang, C.-Y., Chen, W., Su, C.-H., Chang, P.-C., Huang, Y.-T., Hsu, K.-C., Yuan, C.-J., Chang, C.-C., 2019b. *Appl. Phys. Lett.* 114 (9), 093702.
- Chappel, M.C., Ferrario, C.M., 2006. *Kidney Int* 70 (1), 7–9.
- Cheng, T.M., Lee, T.C., Tseng, S.H., Chu, H.L., Pan, J.P., Chang, C.C., 2011. *Nanotechnology* 22 (24), 245105.
- Dong, E., Du, H., Gardner, L., 2020. *Lancet Infect. Dis.* 20 (5), 533–534.
- Donoghue, M., Hsieh, F., Baronas, E., Godbout, K., Gosselin, M., Stagliano, N., Donovan, M., Woolf, B., Robison, K., Jeyaseelan, R., Breitbart, R.E., Acton, S., 2000. *Circ. Res.* 87 (5), E1–E9.
- East, D.A., Mulvihill, D.P., Todd, M., Bruce, I.J., 2011. *Langmuir* 27 (22), 13888–13896.
- Fosbøl, E.L., Butt, J.H., Østergaard, L., Andersson, C., Selmer, C., Kragholm, K., Schou, M., Phelps, M., Gislason, G.H., Gerds, T.A., Torp-Pedersen, C., Køber, L., 2020. *JAMA* 324 (2), 168–177. <https://doi.org/10.1001/jama.2020.11301>.
- Ghosal, S., Mukherjee, J.J., Sinha, B., Gangopadhyay, K.K., 2020. medRxiv. <https://doi.org/10.1101/2020.04.23.20076661>.
- Harrison, C., 2020. *Nat. Biotechnol.* 38 (4), 379–381.
- Hong, R.J., Song, X., Tao, C.X., Zhang, D.H., Zhang, D.W., 2016. *Appl. Phys. A - Mater.* 122 (3), 178.
- Kilic, T., Brunner, V., Audoly, L., Carrara, S., 2018a. *Biosens. Bioelectron.* 100, 139–147.
- Kilic, T., Soler, M., Fahimi-Kashani, N., Altug, H., Carrara, S., 2018b. *Biosensors* 8 (1), 6.
- Li, H.Y., Tseng, S.H., Cheng, T.M., Chu, H.L., Lu, Y.N., Wang, F.Y., Tsai, L.Y., Shieh, J.Y., Yang, J.Y., Juan, C.C., Tu, L.C., Chang, C.C., 2013. *Nanotechnology* 24 (39), 399501.
- Li, S., Liu, J.L., Lu, Y.L., Zhu, L., Li, C.D., Hu, L.J., Li, J., Jiang, J., Low, S., Liu, Q.J., 2018. *Biosens. Bioelectron.* 117, 32–39.
- Lippert, J.L., Tyminski, D., Desmeules, P.J., 1976. *J. Am. Chem. Soc.* 98 (22), 7075–7080.
- Liu, X.-L., Peng, C.-W., Chen, C., Yang, X.-Q., Hu, M.-B., Xia, H.-S., Liu, S.-P., Pang, D.-W., Li, Y., 2011. *Biochem. Biophys. Res. Commun.* 409 (3), 577–582.
- Lundstrom, K., 2017. *Expert Opin. Drug Discov* 12 (4), 335–343.

- Mehta, N., Kalra, A., Nowacki, A.S., Anjewierden, S., Han, Z., Bhat, P., Carmona-Rubio, A.E., Jacob, M., Procop, G.W., Harrington, S., Milinovich, A., Svensson, L.G., Jehi, L., Young, J.B., Chung, M.K., 2020. *JAMA Cardiol* 5 (9), 1020–1026. <https://doi.org/10.1001/jamacardio.2020.1855>.
- Merkle, R.K.W., Pikel, R., Verryn, S.M.C., De Waal, D., 1999. *Miner. Mag.* 63 (3), 363–367.
- Messerli, F.H., Bangalore, S., Bavishi, C., Rimoldi, S.F., 2018. *J. Am. Coll. Cardiol.* 71 (13), 1474–1482.
- Natesh, R., Schwager, S.L., Sturrock, E.D., Acharya, K.R., 2003. *Nature* 421 (6922), 551–554.
- Natesh, R., Schwager, S.L., Evans, H.R., Sturrock, E.D., Acharya, K.R., 2004. *Biochem* 43 (27), 8718–8724.
- Pan, H., Peto, R., Karim, Q.A., Alejandria, M., Henao-Restrepo, A.M., García, C.H., Kiény, M.-P., Malekzadeh, R., Murthy, S., Preziosi, M.-P., Reddy, S., Periago, M.R., Sathiyamoorthy, V., Röttingen, J.-A., Swaminathan, S., 2020. *medRxiv*. <https://doi.org/10.1101/2020.10.15.20209817>.
- Ponikowski, P., Voors, A.A., Anker, S.D., Bueno, H., Cleland, J.G.F., Coats, A.J.S., Falk, V., Gonzalez-Juanatey, J.R., Harjola, V.P., Jankowska, E.A., Jessup, M., Linde, C., Nihoyannopoulos, P., Parissis, J.T., Pieske, B., Riley, J.P., Rosano, G.M.C., Ruilope, L.M., Ruschitzka, F., Rutten, F.H., Meer, P., 2016. *Eur. Heart J.* 37 (27), 2129–2200.
- Ramanavicius, A., Finkelsteinas, A., Cesiulis, H., Ramanaviciene, A., 2010. *Bioelectrochemistry* 79 (1), 11–16.
- Reynolds, H.R., Adhikari, S., Pulgarin, C., Troxel, A.B., Iturrate, E., Johnson, S.B., Hausvater, A., Newman, J.D., Berger, J.S., Bangalore, S., Katz, S.D., Fishman, G.I., Kunichoff, D., Chen, Y., Ogedegbe, G., Hochman, J.S., 2020. *N. Engl. J. Med.* 382 (25), 2441–2448. <https://doi.org/10.1056/NEJMoa2008975>.
- Rocheville, M., Martin, J., Jerman, J., Kostenis, E., 2013. Chapter three - mining the potential of label-free biosensors for seven-transmembrane receptor drug discovery. In: Kenakin, T. (Ed.), *Progress in Molecular Biology and Translational Science*. Academic Press, pp. 123–142.
- Santos, A., Bueno, P.R., Davis, J.J., 2018. *Biosens. Bioelectron.* 100, 519–525.
- Singh, T.U., Parida, S., Lingaraju, M.C., Kesavan, M., Kumar, D., Singh, R.K., 2020. *Pharmacological reports: PR*, pp. 1–30. <https://doi.org/10.1007/s43440-020-00155-6>.
- Sommerstein, R., Kochen, M.M., Messerli, F.H., Gräni, C., 2020. *J. Am. Heart Assoc.* 9 (7), e016509.
- Stewart, S., Fredericks, P.M., 1999. *Spectrochim. Acta A Mol. Biomol. Spectrosc.* 55 (7–8), 1615–1640.
- Tai, W., He, L., Zhang, X., Pu, J., Voronin, D., Jiang, S., Zhou, Y., Du, L., 2020. *Cell Mol. Immunol.* 17 (6), 613–620.
- Tepeli, Y., Ülkü, A., 2018. *Sensor. Actuator. B Chem.* 254, 377–384.
- Tipnis, S.R., Hooper, N.M., Hyde, R., Karran, E., Christie, G., Turner, A.J., 2000. *J. Biol. Chem.* 275 (43), 33238–33243.
- Towler, P., Staker, B., Prasad, S.G., Menon, S., Tang, J., Parsons, T., Ryan, D., Fisher, M., Williams, D., Dales, N.A., Patane, M.A., Pantoliano, M.W., 2004a. *J. Biol. Chem.* 279 (17), 17996–18007.
- Towler, P., Staker, B., Prasad, S.G., Menon, S., Tang, J., Parsons, T., Ryan, D., Fisher, M., Williams, D., Dales, N.A., Patane, M.A., Pantoliano, M.W., 2004b. *J. Biol. Chem.* 279 (17), 17996–18007.
- Tuma, R., 2005. *J. Raman Spectrosc.* 36 (4), 307–319. <https://doi.org/10.1002/jrs.1323>.
- Wan, Y., Shang, J., Graham, R., Baric, R.S., Li, F., 2020. *J. Virol* 94 (7), e00127–20. <https://doi.org/10.1128/jvi.00127-20>.
- Waterhouse, A., Bertoni, M., Bienert, S., Studer, G., Tauriello, G., Gumienny, R., Heer, F. T., de Beer, T.A.P., Rempfer, C., Bordoli, L., 2018. *Nucleic Acids Res* 46 (W1), W296–W303.
- Xu, L.G., Yan, W.J., Ma, W., Kuang, H., Wu, X.L., Liu, L.Q., Zhao, Y., Wang, L.B., Xu, C.L., 2015. *Adv. Mater.* 27 (10), 1706.
- Xu, X.T., Chen, P., Wang, J.F., Feng, J.N., Zhou, H., Li, X., Zhong, W., Hao, P., 2020. *Sci. China Life Sci.* 63, 4.
- Zhao, Y., Zhao, Z., Wang, Y., Zhou, Y., Ma, Y., Zuo, W., 2020. *bioRxiv*. <https://doi.org/10.1101/2020.01.26.919985>.
- Zheng, Y.Y., Ma, Y.T., Zhang, J.Y., Xie, X., 2020. *Nat. Rev. Cardiol.* 17 (5), 259–260.
- Zhu, C.J., Tong, N., Song, L.X., Zhang, G.Q., 2015. In: Zhou, Zhiping (Ed.), *International Symposium on Photonics and Optoelectronics 2015*, 9656. SPIE, 96560E, 10.1117/12.2205157.